Contactless Current Measurement for Enclosed Multiconductor Systems Based on Sensor Array

Guangchao Geng, *Member, IEEE*, Juncheng Wang, *Student Member, IEEE*, Kun-Long Chen, *Member, IEEE*, and Wilsun Xu, *Fellow, IEEE*

***Abstract*— How to measure ac currents in a bundle of inaccessible, enclosed conductors has been a challenging problem but with many potential applications. This paper presents a method to solve the problem using an array of magnetic field sensors. The proposed method consists of two novel ideas. The first idea is to use an off-site calibration method to establish sensor parameters including sensing position and angle, which provides more accurate sensor parameter estimation than their nominal values. The second idea is to "measure" (i.e., calculate) conductor currents and positions based on the sensed magnetic fields and preestablished sensor parameters. This process is simplified since the sensor information is obtained by the first idea. Both calibration and measurement tasks are formulated as nonlinear least square problems and solved efficiently. The proposed method is demonstrated for the cases involving ideal three-conductor system and practical residential service cable enclosed in a plastic conduit. The method has the potential for contactless current measurement of Romex cables and overhead distribution lines.**

***Index Terms*— Calibration, current measurement, multiconductor systems, nonlinear least square (NLLS), sensor array.**

NOMENCLATURE

Set and Dimension

$\mathbb{S}_S, n_S$	Magnetic sensors.
$\mathbb{S}_C, n_C$	Calibrating conductors.
$\mathbb{S}_I, n_I$	Conductors to be measured.
n, m	Unknown parameters and observations in nonlinear least square (NLLS).

Conductor System

x_C, y_C	Coordinate of calibrating conductor.
x_I, y_I	Coordinate of conductor to be measured.
I	Current.
D, d	Diameter of cable and its internal conductor.
R_I	Radius of enclosing conduit.

Sensor System

x_S, y_S	Coordinate of sensor.
θ	Sensing directional angle.
ρ, ϕ	Gain factor and phase shift.
B	Magnetic flux density.
V	Output voltage of a sensing system.
R_S	Sensor position mismatch tolerance.
r, δ	Position and angular distance between conductor and sensor.

Misc

μ_0	Magnetic permeability.
$\hat{(\cdot)}$	Phasor.
$(\cdot)_r + \mathbf{i}(\cdot)_i$	Real and imaginary part of a phasor.
$\overline{(\cdot)}$	Reference values.

Manuscript received October 25, 2016; revised January 20, 2017; accepted April 3, 2017. Date of publication June 22, 2017; date of current version September 13, 2017. The Associate Editor coordinating the review process was Dr. Branislav Djokic. This work was supported in part by the National Natural Science Foundation of China under Grant 51607155, in part by the China Post-Doctoral Science Foundation under Grant 2015M570506, and in part by the China Post-Doctoral Council under Grant 20150004. *(Corresponding author: Guangchao Geng.)*

G. Geng is with the College of Control Science and Engineering, Zhejiang University, Hangzhou 310027, China (e-mail: ggc@zju.edu.cn).

J. Wang, K.-L. Chen, and W. Xu are with the Department of Electrical and Computer Engineering, University of Alberta, Edmonton, AB T6G 2R3, Canada.

Color versions of one or more of the figures in this paper are available online at http://ieeexplore.ieee.org.

Digital Object Identifier 10.1109/TIM.2017.2711898

I. INTRODUCTION

CURRENT sensing is one of the basic measurement techniques for modern power systems, ranging from residential, industrial to utility practices [1]. How to measure currents in a bundle of conductors enclosed in a structure has been a challenging task but with great potential applications. For example, Romex cable has two or three conductors enclosed in a plastic cover. It has been difficult to measure the currents of these conductors without isolating the conductors first. A method to estimate currents for such cables using external sensors was patented [2]. Contactless measurement of overhead line currents encounter similar challenges. In this case, magnetic fields measured by an array of sensors are used to estimate currents of distribution feeders [3]. Recently, the need to monitor home energy use by home owners has motivated the research on measuring currents in three conductors enclosed in a plastic conduit [4], as a key enabling technique for nonintrusive load monitoring (NILM) [5].

All of the above research works and potential applications share a common characteristic, namely, measuring currents on conductors that cannot be accessed individually. This problem is illustrated using Fig. 1. In this figure, a set of magnetic field sensors are around the conduit. The goal is to determine conductor currents inside the conduit using sensor data and without knowing conductor positions.

Magnetic sensors [6], including coil [7], [8] and Hall effect-based sensors [9], [10], were utilized to measure magnetic fields and identify currents. Sensor array-based approaches were developed in order to make use of spatial difference and measuring redundancy of multiple sensors to achieve

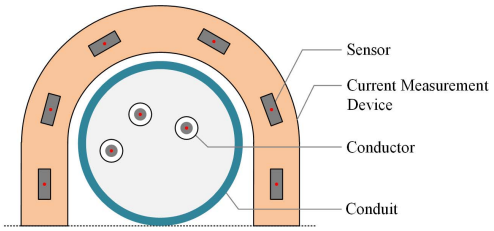

Fig. 1. System scheme of sensor array for enclosed multiconductor system.

better performance [11]. Libove and Singer formulates the contactless current measurement problem as an optimization problem determining current values using a high number of sensors, which are infeasible to be on a device with limited physical size. Bourkeb *et al.* and AVO International Ltd. implement current measurement for two or three conductors based on the preassumed conductor geometric information from user selected Romex cable specification, which leads to large measuring errors and withdrawn products. Gao *et al.* proposed an on-site calibration method to establish the relationship of conductor currents and magnetic fields. A dedicated calibration device that draws currents from the conductors downstream of the sensing point was developed. The method is limited to the situations where the conductors are accessible so that the calibrating signals can be injected. For example, the method is unable to measure overhead conductor currents.

The objective of this paper is to present an improved method to solve the problems above. The method consists of two ideas. The first idea is to use an off-site calibration method to find out sensor electrical and geometric parameters; these parameters have strong impact on the current measurement accuracy. The second idea is solve the currents (and positions) of the conductors based on the calibrated parameters above and the measured magnetic flux density data. This approach does not rely on any preassumption of conductor configuration. It is, therefore, applicable to various scenarios of current measurement, such as the cases of Romax cables, conductors enclosed in a conduit, and overhead distribution lines.

II. Contactless Current Measurement

A. Sensing Principle

An ideal straight conductor with ac current produces an alternating magnetic field around it. This magnetic field can be captured by magnetic sensors like coils. Fourier transformation is performed to convert time-domain sensor signals to base frequency phasors. A phasor-based representation of magnetic flux density $\hat{B}$ at a point with position and angular distance r and δ to the conductor with current $\hat{I}$ is obtained as

$$\hat{B} = \frac{\mu_0 \cos\delta}{2\pi r}\hat{I}. \tag{1}$$

A voltage is induced on the coil sensor by the projection of the magnetic flux density onto the sensing direction as shown in Fig. 2. This voltage signal is amplified by an analog circuit

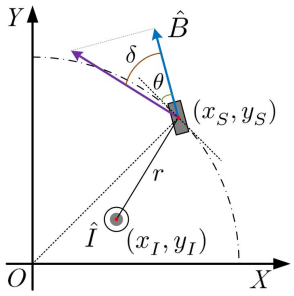

Fig. 2. Geometry modeling of sensor and conductor.

with output voltage $\hat{V}$, then digitalized by analog-to-digital converter (ADC), and finally recorded for analytics.

The effect of coil sensor induction and amplifier circuit can be modeled using a gain factor ρ and a phase shift ϕ as

$$\hat{V} = \rho e^{\mathbf{i}\phi}\hat{B} = \rho e^{\mathbf{i}\phi}\frac{\mu_0 \cos\delta}{2\pi r}\hat{I}. \tag{2}$$

Given all the parameters involved, one is able to reversely derive the current $\hat{I}$ using the measured voltage $\hat{V}$.

B. Enclosed Multiconductor System and Sensor Array

For an enclosed multiconductor system shown in Fig. 1, in order to completely recover all the currents, an array of sensors are on a plane that is perpendicular to the conductors. Then, the output voltage signals are recorded simultaneously, for the use of solving current values.

One of the unique challenges in contactless current measurement is that the distance r and angle δ between the studied conductors and sensors are practically unknown. r and δ can be expressed using Cartesian coordinates, shown in Fig. 2. Then, the output voltage phasor $\hat{V}_k$ is basically a nonlinear function of all present currents and parameters shown at the bottom of the page, where (x_S^k, y_S^k) and (x_I^j, y_I^j) are the coordinates of kth sensor and ith conductor, respectively.

C. Application Example: Home Energy Use Monitoring

One of the important application scenarios for contactless current measurement is home energy use monitoring, shown in Fig. 3. The sensing device is installed around the plastic conduit outside incoming wires of household electrical panels. Three conductors, including two hot wires ($\pm$110 V ac) and one neutral wire, are enclosed. Both positions and currents of three conductors are to be determined. The measured currents can be used in many applications such as energy use estimation or NILM. According to the existing investigations on magnetic sensor array-based approach [14] and clamp-on current probe-based approach [15] for home energy use monitoring, current measurement accuracy within 5% is required to provide sufficiently accurate estimation for home energy consumption.

$$\hat{V}_k = \sum_{j\in\mathbb{S}_I} \frac{\mu_0\rho_k e^{\mathbf{i}\phi_k}}{2\pi}\hat{I}_j \frac{\left(\left(x_S^k\cos\theta_k - y_S^k\sin\theta_k\right)\left(x_S^k - x_I^j\right) + \left(y_S^k\cos\theta_k + x_S^k\sin\theta_k\right)\left(y_S^k - y_I^j\right)\right)}{\sqrt{\left(x_S^k\right)^2 + \left(y_S^k\right)^2}\left(\left(x_S^k - x_I^j\right)^2 + \left(y_S^k - y_I^j\right)^2\right)} \quad k \in \mathbb{S}_S \tag{3}$$

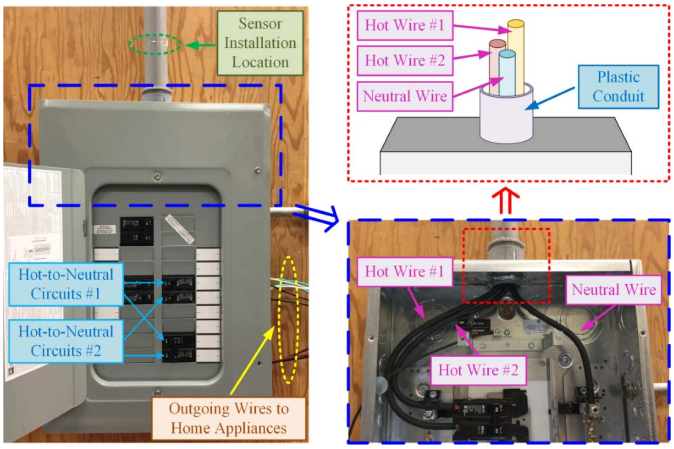

Fig. 3. Household electrical panel in North American homes.

D. Proposed Measurement Idea

The problem as described in Section II-B is restated as follows: solve for conductor currents with measured magnetic fields. Such a problem is unsolvable since both sensor and conductor positions are unknown, namely, there are more unknowns than available equations. Increasing the number of sensors can establish more equations but it also introduces more unknown sensor positions. In this paper, we recognize that sensor parameters are the property of sensing device and are independent of conductor configurations. It is, therefore, sensible to first determine sensor positions and orientations with respect to a reference point. Once the sensor parameters are obtained, the problem of "measuring" conductor currents then becomes solvable. In addition, adding more sensors leads to redundant equations for improved accuracy.

Determining sensor parameters is, unfortunately, not a simple task. First, it is very difficult, if not impossible, to install sensors at precise positions and with desired orientations. It is even more difficult to measure sensor positions and angles using mechanical means. Second, each sensor has an amplifier circuit, whose gain factor and phase shift must be established as well. Otherwise, additional unknown variables are introduced. In view of these challenges, we propose to use an electrical method to determine sensor parameters. This method, called sensor calibration, is to let each sensor to measure the magnetic fields of a set of conductors with precisely known positions and currents. The sensor parameters are solved from the resultant equations. This off-site calibration process can be done as a part of the manufacturing process of the measurement device. Once a device is assembled, it is mounted onto a calibrator; the outputs of all sensors are collected. Then the sensor parameters are solved and burned into an EPROM embedded in the device. Thus, each device has its own sensor parameters established regardless of the precision of sensor installation.

Once sensor parameters become available, the device will be able to measure currents of various conductor configurations. This is the problem of solving conductor currents and positions based on known sensor parameters and outputs. An NLLS is utilized to solve this problem. NLLS performs nonlinear regression with m observations and n unknown parameters ($m \geq n$). It is a special form of nonlinear programming (NLP). In fact, the sensible calibration is also formulated as an NLLS problem, resulting in consistent solutions to both calibration and measurement problems.

III. Off-Site Sensor Calibration

A. Principle and Method

The goal of sensor calibration is to find the sensor-specific parameters, including ρ_k, ϕ_k, x_S^k, y_S^k, and θ_k for kth sensor. The idea is to use a set of measured currents with known positions to determine sensor parameters by measuring calibrating current and sensor output voltages simultaneously. In order to simplify the process and avoid interconductor interference, only one conductor is used for each calibrating process.

The following n_C times of single conductor calibrating experiments are performed, which constitute the set of calibration data set $\mathbb{S}_C$. A single conductor with an ac current measured by current probe is placed straightly at a specified location inside the conduit with known position.

B. Calibration Data Processing

Calibration is done sensor by sensor. For kth sensor, phase shift ϕ_k can be first determined as the average angular difference between measured current and voltage phasor as (4). Note that we use the subscript $(\cdot)_q$ to refer to current and voltage obtained in the calibration stage. For jth calibrating experiment, the output voltages of all sensors ($\hat{V}_q^{j,k}, k \in \mathbb{S}_S$) are recorded simultaneously with the calibrating current $\hat{I}_q^j$ on the conductor at position $(\overline{x_C^j}, \overline{y_C^j})$

$$\phi_k = \frac{1}{n_C} \sum_{j \in \mathbb{S}_C} \left(\angle \hat{V}_q^{j,k} - \angle \hat{I}_q^j \right). \tag{4}$$

After obtaining ϕ_k, the remaining parameters are able to be calibrated using the magnitudes of measured phasors, i.e., I_q^j and $V_q^{j,k}$, based on the NLLS formulation shown at the bottom of the page. Auxiliary variables $V_t^{j,k}$ are used to reduce the nonlinearity in (3), as shown at the bottom of the previous page, which is representing output voltage on kth sensor caused by jth calibrating experiment with conductor position $(\overline{x_C^j}, \overline{y_C^j})$. Also, multiple inequality constraints are considered for better optimum searching. Physical sensor position $(\overline{x_S^k}, \overline{y_S^k})$ is used as a reference, the calibrated position is constrained in a circle with tolerance radius R_S. Note that, if calibrating conductors are distributed on the two sides of the line along sensing direction, one has to first correct the opposite directions of voltage phasors before applying (4). Negative values of $V_q^{j,k}$ are expected in this case.

Therefore, parameters for kth sensor ρ_k, θ_k, x_S^k, and y_S^k are found by solving NLLS problem (5), as shown at the top of the next page. Since there are essentially four independent unknown parameters (i.e., $n = 4$), one has to obtain at least four sets of observations (i.e., $m \geq n$) to fully determine the unknowns. Using redundant calibration data samples is able to improve the accuracy of calibrating parameters. The optimal number of calibrating experiments (i.e., n_C) is investigated in Section VI-B.

$$\min\ \psi_k\left(x_S^k, y_S^k, \rho^k, \theta^k, V_t^{j,k}\right)\big|_{j\in\mathbb{S}_C} = \sum_{j\in\mathbb{S}_C}\left(V_t^{j,k} - V_q^{j,k}\right)^2$$

$$\text{s.t.}\ \begin{cases} \rho_{\min}^k \le \rho_k \le \rho_{\max}^k \\ \theta_{\min}^k \le \theta_k \le \theta_{\max}^k \\ 0 \le \left(x_S^k - \overline{x_S^k}\right)^2 + \left(y_S^k - \overline{y_S^k}\right)^2 \le R_S^2 \\ \forall j \in \mathbb{S}_C \ \begin{cases} -V_{\max}^k \le V_t^{j,k} \le V_{\max}^k \\ \dfrac{\mu_0}{2\pi}\rho_k I_m^j\left(\left(x_S^k\cos\theta_k - y_S^k\sin\theta_k\right)\left(x_S^k - \overline{x_C^j}\right) + \left(y_S^k\cos\theta_k + x_S^k\sin\theta_k\right)\left(y_S^k - \overline{y_C^j}\right)\right) \\ -V_t^{j,k}\sqrt{\left(x_S^k\right)^2 + \left(y_S^k\right)^2}\left(\left(x_S^k - \overline{x_C^j}\right)^2 + \left(y_S^k - \overline{y_C^j}\right)^2\right) = 0 \end{cases} \end{cases} \tag{5}$$

$$\min\ \psi\left(x_I^j, y_I^j, I_r^j, I_i^j, V_r^{j,k}, V_i^{j,k}\right)\big|_{j\in\mathbb{S}_I, k\in\mathbb{S}_S} = \sum_{k\in\mathbb{S}_S}\left(\left(V_{c,r}^k - \sum_{j\in\mathbb{S}_I} V_r^{j,k}\right)^2 + \left(V_{c,i}^k - \sum_{j\in\mathbb{S}_I} V_i^{j,k}\right)^2\right)$$

$$\text{s.t.}\ \begin{cases} \forall j \in \mathbb{S}_I \ \begin{cases} -I_{\max}^j \le I_r^j \le I_{\max}^j, \quad -I_{\max}^j \le I_i^j \le I_{\max}^j \\ 0 \le \left(x_I^j\right)^2 + \left(y_I^j\right)^2 \le R_I^2 \end{cases} \\ \forall j \in \mathbb{S}_I \\ \forall k \in \mathbb{S}_S \end{cases} \ \begin{cases} -V_{\max}^k \le V_r^{j,k} \le V_{\max}^k, \quad -V_{\max}^k \le V_i^{j,k} \le V_{\max}^k \\ \dfrac{\mu_0}{2\pi}\rho_k I_r^j\left(\left(x_S^k\cos\theta_k - y_S^k\sin\theta_k\right)\left(x_S^k - x_I^j\right) + \left(y_S^k\cos\theta_k + x_S^k\sin\theta_k\right)\left(y_S^k - y_I^j\right)\right) \\ \qquad -V_r^{j,k}\sqrt{\left(x_S^k\right)^2 + \left(y_S^k\right)^2}\left(\left(x_S^k - x_I^j\right)^2 + \left(y_S^k - y_I^j\right)^2\right) = 0 \\ \dfrac{\mu_0}{2\pi}\rho_k I_i^j\left(\left(x_S^k\cos\theta_k - y_S^k\sin\theta_k\right)\left(x_S^k - x_I^j\right) + \left(y_S^k\cos\theta_k + x_S^k\sin\theta_k\right)\left(y_S^k - y_I^j\right)\right) \\ \qquad -V_i^{j,k}\sqrt{\left(x_S^k\right)^2 + \left(y_S^k\right)^2}\left(\left(x_S^k - x_I^j\right)^2 + \left(y_S^k - y_I^j\right)^2\right) = 0 \end{cases} \tag{7}$$

IV. On-Site Current Measurement

A. Preprocessing

In measurement stage, the sensing device is allocated outside the enclosed conduit as Fig. 1. The aim of measurement stage is to find the accurate currents and positions of n_I conductors in the set of $\mathbb{S}_I$ inside the enclosed conduit, based on the information of n_S sensor output voltages in the set of $\mathbb{S}_S$. Necessary preprocessing procedures related to sensor-circuit response have to be performed as follows. Note that we use the subscripts $(\cdot)_p$ and $(\cdot)_c$ to denote measured and preprocessed voltage phasors in the on-site measurement stage.

Parameter ϕ_k describes the phase delay effect of the output voltage $\hat{V}_p^k$ with respect to its inducing magnetic field shown in (2), such phase delay can be compensated before determining currents. Given the calibrated ϕ_k obtained by (4) in calibration stage, phase-compensated voltage phasor $\hat{V}_c^k$ is obtained using

$$V_{c,r}^k + \mathbf{i}V_{c,i}^k = e^{-\mathbf{i}\phi_k}\hat{V}_p^k \tag{6}$$

where $V_{c,r}^k$ and $V_{c,i}^k$ refer to real and imaginary parts of $\hat{V}_c^k$, which will be used in NLLS formulation shown at the bottom of the page instead of the measured $\hat{V}_p^k$.

B. Measurement Formulation

The current measurement formulation is based on NLLS (7), as shown at the top of this page, which utilizes the following data: sensor geometrical parameters (x_S^k, y_S^k, $and\theta_k$) and electrical parameters (ρ_k) from the calibration result in Section III, as well as phase-compensated voltages ($V_{c,r}^k + \mathbf{i}V_{c,i}^k$) from preprocessing in Section IV-A.

In this formulation, position (x_I^j, y_I^j) and current in phasor form ($I_r^j + \mathbf{i}I_i^j$) of all conductors are to be determined, which essentially follow the nonlinear equation (3). The objective function is to minimize absolute mismatches between measured and calculated sensor output voltages. Using absolute mismatches, measurements of small magnitude are with proportional small weight, since they are commonly with large relative error that has to be eliminated.

Boundary constraints are enforced for each variable, where $V_{\max}^k$ is set as the voltage measurement range of ADC module and $I_{\max}^j$ is set as the rated current capacity of the conductor. Conductors are possibly anywhere within the conduit with radius R_I, so a corresponding geometry constraint is added.

Phasor-based auxiliary variables $V_r^{j,k} + \mathbf{i}V_i^{j,k}$ are inserted into (7), representing the voltage components from kth sensor caused by jth conductor, in order to reduce the nonlinearity after rearrangement of the NLLS formulation.

C. Auxiliary Constraints

1) Net Current Constraint: In some circumstances, net current of the studied conductor set can be known beforehand or easily measured as ($I_{n,r} + \mathbf{i}I_{n,i}$) by adding a clamp-on

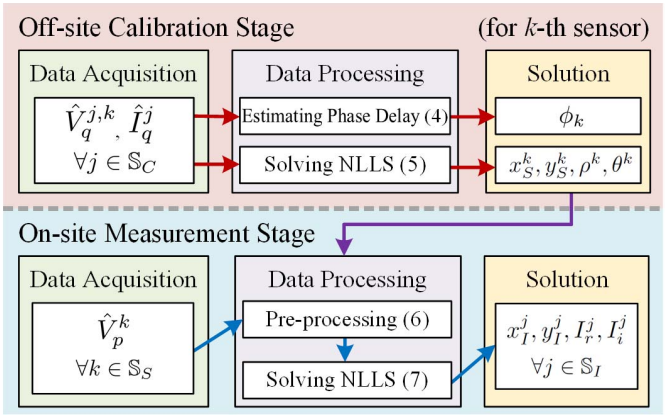

Fig. 4. Flowchart of the proposed two-stage current sensing approach.

ac current probe on the conduit. The following constraint can be added into (7) to assist optimum searching:

$$\sum_{j\in\mathbb{S}_I} I_r^j = I_{n,r}, \quad \sum_{j\in\mathbb{S}_I} I_i^j = I_{n,i}. \tag{8}$$

2) Cable Geometry Constraints: For the cases that the geometry distances of conductors are known *a priori*, especially for cables with marked model and available specification, one is able to integrate the following constraint into the NLLS formulation (7) in order to specify the relative position of conductors, where D and d are the external diameter of the cable and the diameter of internal conductors inside the cable, respectively:

$$d^2 \le \left(x_I^{j_1} - x_I^{j_2}\right)^2 + \left(y_I^{j_1} - y_I^{j_2}\right)^2 \le D^2 \quad \forall j_1, j_2 \in \mathbb{S}_I, \ \ j_1 \ne j_2. \tag{9}$$

V. Procedure Flowchart

As a brief summary of the proposed two-stage contactless current measurement approach, a procedure flowchart is provided as shown in Fig. 4. We are able to clearly see that the off-site calibration stage is based on calibrating data set $\mathbb{S}_C$ to determine sensor parameters. The resultant sensor parameters are used in current measurement stage along with sensor output voltages $\hat{V}_p^k$ to find out conductor positions (x_I^j, y_I^j) and current values (I_r^j, I_i^j) in the enclosed conduit.

Note that once the calibration procedures are conducted, the calibrated sensor parameters are completely decoupled with conductor systems and stored in an embedded memory, they are valid for multiple current measurement operations and various types of multiconductor systems.

VI. Case Studies

A. Test Bed and Implementation

Laboratory experiments have been performed to validate the effectiveness of the proposed approach on a test bed shown in Fig. 5. The schematic is visualized in Fig. 6. The overall dimensions of the U-shaped sensing device are $10 \times 4 \times 7$ cm ($l \times w \times h$). The inner diameter is 44 mm to accommodate the conductor holder and the conduit.

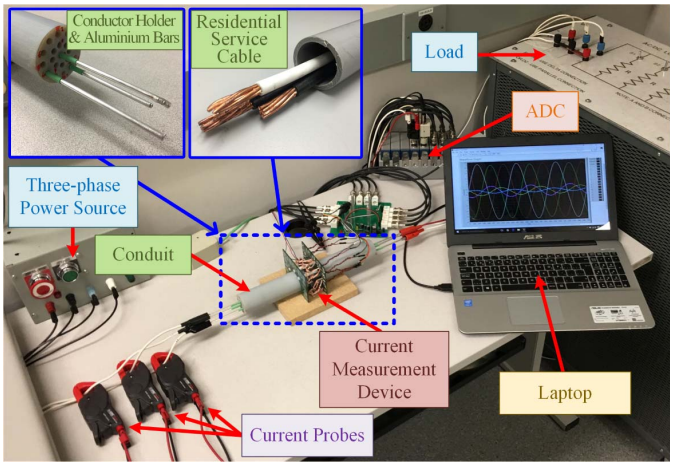

Fig. 5. Test bed of contactless current measurement.

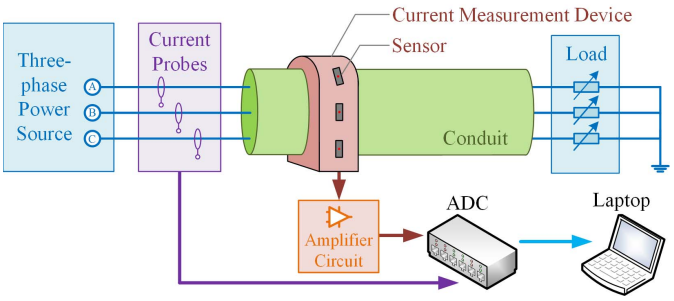

Fig. 6. Schematic of the test bed.

The reference currents are obtained using a three-phase power source and a set of adjustable loads, connected by a testing conductor set inside a polyvinyl chloride conduit, on which the sensing device is installed. The reference current values are measured using AEMC MN252 current probes [16] on each individual conductor, for both calibration and measurement stages. The current magnitude and phase accuracy of the current probe is 2.5% of the reading ± 5mV and ≤5.0°, respectively (its output ratio is 10 mV/A). Balanced and unbalanced currents with different magnitudes are obtained using different load combinations for each phase, in order to emulate practical operation currents.

Six pairs of two-axis coil sensors are installed around the conduit as a semicircle perpendicular to the conductors, shown in Figs. 1 and 6. Each cylinder-shaped coil sensor is 5 mm in diameter and 8 mm in length. To save space of printed circuit board (PCB), a pair of sensors is embedded in a sensor holder and positioned in different sensing directions perpendicular to the conductors. The sensor holders are installed on the PCB. Geometrical layout of the sensors is demonstrated in the calibration result in Section VI-B. Small position mismatches caused by manual sensor installation are observed in the sensor pairs, and these mismatches are identified in the off-site calibration and will not affect the accuracy performance of on-site current measurement.

All the measurements, including currents and sensor output voltages, are acquired using a National Instrument CompactDAQ with four 9215 simultaneous analog input modules and recorded by a laptop with LabVIEW data acquisition software.

The ADC modules used in the test bed are with ±10-V range and 16-b resolution. The minimum recognizable signal step is $[(2 \times 10\ \text{V})/2^{16}] = 0.31$ mV. The developed algorithm processes sensor signals to calculate currents and compare them with the reference ones.

Two types of enclosed multiconductor systems were tested as shown in Fig. 5. The first one is straight aluminum round rods with diameter 3.618 mm installed on a conductor holder with 21 known positions. It is used to obtain calibration data and evaluate sensor error. The second one is a three-conductor residential service cable with individual conductor diameter around 7 mm, the conductors are not strictly straight and perpendicular to the sensing device. This is used to emulate practical situations that go beyond ideal assumptions.

The NLLS formulation is implemented in AMPL [17] and solved using KNITRO [18] as the optimizer. Interior point method is selected to solve the formulated NLP problems. The computing performance data is obtained using a laptop with Intel Core i7-2860QM 2.50-GHz CPU.

This paper is focusing on the three-conductor problem and semicircular configuration of coil sensors. However, it is expected to be applicable for other conductor and sensor arrangements, like two-wire problem [19], due to the flexible nature of NLLS as a constrained nonlinear optimization problem. Based on the NLLS formulation, one is able to easily customize reinforcing constraints like (8)–(9), as well as scale up the formulation for additional sensors and conductors.

In the following discussion, currents and voltages are shown in peak values instead of root mean square values, in order to be consistent with phasor representation used above.

B. Calibration of Sensor Parameters

1) Determining n_C: One has to determine n_C before calibration, that is, how many calibrating samples are sufficient to obtain sensor parameters that are accurate enough. Theoretically, an NLLS problem is able to be solved if the number of observations (m) is no less than the number of unknown parameters (n), i.e., $m \geq n$. In this case, four sets of calibrating measurements are sufficient to determine the four sensor parameters (i.e., ρ_k, ϕ_k, x_S^k, and y_S^k). However, in practice, redundant measurements are preferred since uncertainties always exist. Regression using exact number of observations leads to poor calibration results. In order to find a proper n_C setting, Fig. 7 illustrates the norm of mismatches between calculated and measured sensor outputs, i.e., objective values in NLLS formulation (5). Calibrated and uncalibrated conductors refer to the conductor positions that are used and not used in calibration, respectively. The algorithm is actually fitting local error when only four conductors are used for calibration and is leading to a significant global error. Meanwhile, the algorithm is able to reduce global error when 10 or more calibrating conductors are used. However, increasing n_C greater than 10 does not reduce calibration error level. Hence, n_C is selected as 10 for the studied sensing system as a proper setting value.

2) Evaluating Errors: The voltage values in calibration range from 0.01 to 6 V. Absolute and relative errors between

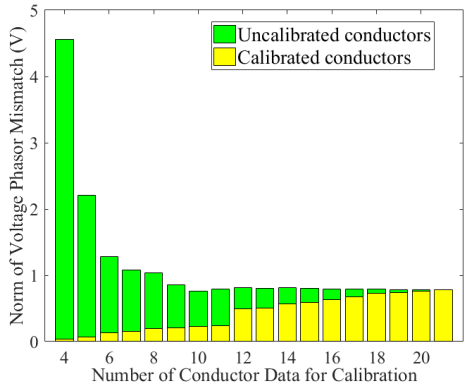

Fig. 7. Determining n_C by evaluating local and global calibration errors.

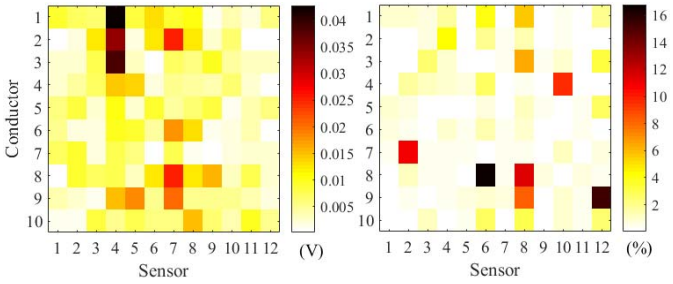

Fig. 8. Absolute and relative mismatches between measured and calculated calibration voltage data $V_t^{j,k}$.

calculated and measured sensor outputs have to be evaluated and checked after calibration, which are visualized using color maps shown in Fig. 8 and can be used for diagnosing the sensing device. If apparent large values are found in a row or column, it indicates an erroneous calibrating data sample or a flawed sensor, respectively. If the errors are averagely distributed and with small values, just as shown in Fig. 8, then it is convinced that an accurate calibration result is obtained.

3) Calibration Results: The calibration result of the sensing device used in this paper is shown in Fig. 9, where the circles and squares refer to the calibrating conductor positions and the calibrated sensor positions, respectively. The short lines across the sensors indicate their sensing directions. Small spacing between the positions of sensor pairs are observed; this indicates that the mismatches in manual sensor installation in the two-axis sensor holder are identified in the calibration stage. Such mismatches will not affect the accuracy of on-site current measurement.

C. Current Measurement Using Ideal Conductors

Ideal conductors refer to the test cases that the aluminum rods are placed straightly on the conductor holder, so that the conductor position can be estimated approximately.

A step-by-step description on current measurement is provided below using a typical test case based on ideal conductors (i.e., Case 5 with balanced three-phase current in Table I). The time-domain signals obtained from sensing device are shown in Fig. 10, where the currents are used for reference. Fourier transformation is performed to obtain phasors in base

TABLE I
CURRENT MEASUREMENT RESULTS WITH IDEAL CONDUCTORS

Conductors	Case	E_V (mV)	E_V%	E_I (A)	E_I%	E_P (deg)
Balanced Scattered	1	52.76	4.17%	0.46	1.95%	1.14°
	2	51.29	3.63%	0.38	1.63%	0.29°
	3	38.05	6.12%	0.51	2.17%	0.86°
	4	46.12	3.65%	0.44	1.89%	1.01°
Balanced Gathered	5	28.37	8.69%	0.58	2.45%	0.60°
	6	37.89	5.99%	0.52	2.22%	0.64°
	7	76.21	8.14%	0.60	2.55%	1.63°
	8	83.05	8.45%	0.54	2.28%	2.04°
Unbalanced Scattered	1	36.92	9.23%	0.53	2.57%	2.34°
	2	47.22	4.31%	0.48	2.03%	0.51°
	3	44.72	5.40%	0.39	1.88%	0.61°
	4	44.85	9.90%	0.67	2.83%	2.35°
Unbalanced Gathered	5	57.56	8.14%	0.25	2.11%	2.28°
	6	32.62	3.89%	0.57	2.78%	1.28°
	7	60.60	8.96%	0.33	1.51%	0.71°
	8	75.05	9.41%	0.56	2.68%	2.15°

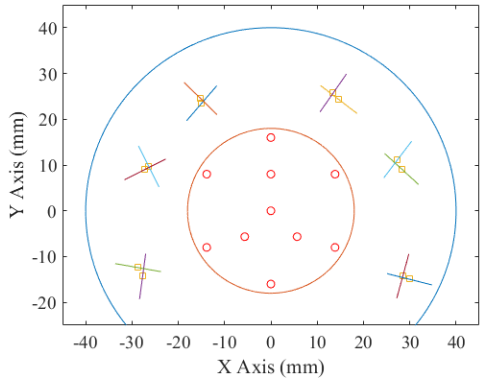

Fig. 9. Calibrating conductor positions and calibrated sensor positions.

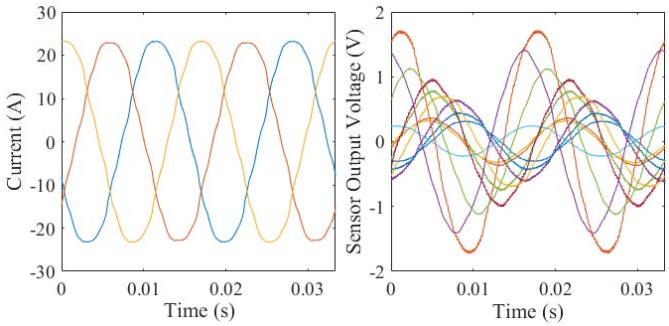

Fig. 10. Waveform samples of currents and sensor output voltages.

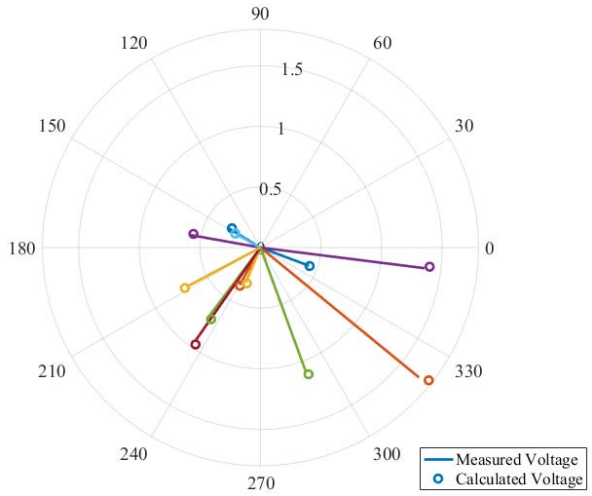

Fig. 11. Measured and calculated sensor output voltages (angle in degree and magnitude in volt).

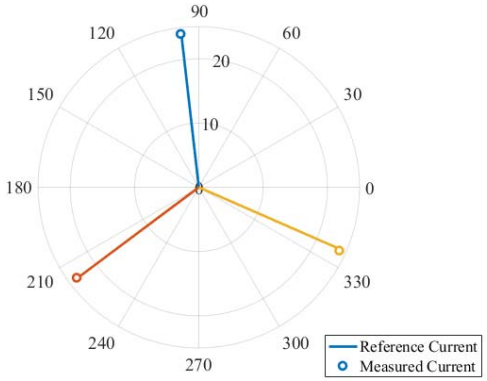

Fig. 12. Measurement result: current phasors (angle in degree and magnitude in ampere).

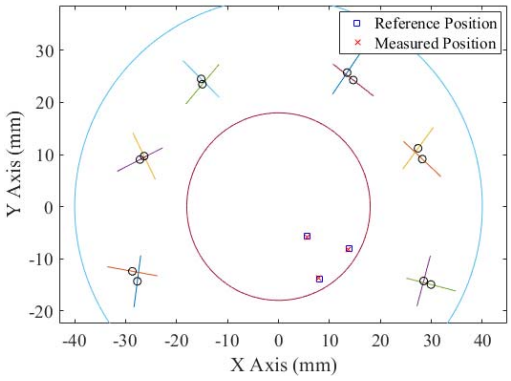

Fig. 13. Measurement result: conductor positions.

frequency and filter out distortions, shown in Fig. 11. The calculated voltages refer to the ones computed using (3) based on known current and conductor position information. Small mismatches are observed between the calculated and measured voltages shown in Fig. 11, which are caused by two major categories of uncertainties: nonideal sensor measurement and imperfect calibration solution. The former one causes error in measured voltage phasors, while the later one leads to inaccurate calculated phasors. A detailed analysis is provided in Section IV-E to address these uncertainty issues. These sensor signals are processed by the proposed algorithm to identify conductor currents as well as positions, taking advantage of redundant sensor array measurements. The measurement result is shown in Figs. 12 and 13. Acceptable errors are found in both conductor positions and currents.

In order to perform a complete benchmark, two typical conductor configurations, namely, gathered and scattered cases, are tested with balanced and unbalanced three-phase currents shown in Table I. For gathered cases, conductors are allocated close to each other with minimum distance around 7 mm.

TABLE II
CURRENT MEASUREMENT RESULTS USING DIFFERENT CURRENT VALUES

Reference Current (A)	E_V (mV)	$E_V\%$	E_I (A)	$E_I\%$	E_P (deg)
2.01	3.59	12.51%	0.14	6.96%	2.41°
4.06	9.10	8.46%	0.25	6.46%	2.85°
6.08	14.74	8.65%	0.34	5.83%	2.93°
12.11	31.27	8.86%	0.25	2.09%	2.95°
17.96	46.93	9.01%	0.40	2.22%	2.09°
23.73	61.74	8.97%	0.58	2.43%	2.29°

TABLE III
MEASUREMENT RESULTS FOR RESIDENTIAL SERVICE CABLE WITH/WITHOUT CABLE GEOMETRY CONSTRAINTS (9)

Current Config.	Case	w/o Const. (9)			w/ Const. (9)		
		E_I (A)	$E_I\%$	E_P (deg)	E_I (A)	$E_I\%$	E_P (deg)
Balanced	1	1.88	8.03%	3.61°	0.90	3.85%	3.54°
	2	1.05	4.43%	4.09°	0.43	1.81%	1.41°
	3	0.57	2.41%	1.96°	0.57	2.41%	1.96°
	4	0.79	3.34%	2.04°	0.54	2.26%	1.52°
Unbalanced	1	1.38	6.68%	3.03°	0.73	3.51%	2.94°
	2	0.78	3.70%	3.53°	0.23	1.10%	1.29°
	3	0.54	2.60%	1.85°	0.54	2.60%	1.85°
	4	0.88	3.73%	2.59°	0.65	3.09%	1.25°

For scattered cases, conductors are with larger distance of more than 12 mm. Reference currents are around 24 A. Maximum absolute and relative magnitude errors between measured and calculated sensor output voltages (E_V, $E_V\%$) as well as currents (E_I, $E_I\%$) are used as indices to evaluate the measurement accuracy. Maximum phase errors between measured and calculated currents (E_P) are also presented. E_V and $E_V\%$ represent the measurement quality of sensors, while E_I, $E_I\%$, and E_P indicate the performance of current measurement. According to the measurement results, given unneglectable individual sensor errors above 8% for $E_V\%$, the proposed approach is able to maintain current magnitude error below 3% and phase error below 3°, which are close to the accuracy specification of the reference current probes.

Measurement results with different current values are also investigated in Table II, based on a gathered conductor configuration (i.e., Case 8 in Table I). Balanced reference currents are changed from 2 to 23 A. Current magnitude error ($E_I\%$) decreases below 3% when reference currents are larger than 10 A, while the maximum phase error is below 3° given different reference currents. Multiple uncertainty factors contribute to this phenomenon, which will be discussed in Section VI-E. Such measurement accuracy performance is considered to be acceptable for the application requirement of home energy use monitoring shown in Section II-C, since large current scenarios actually dominate the overall household energy consumption.

D. Current Measurement Using Residential Service Cable

Current measurement results for residential service cable with and without geometry constraints (9) are shown in Table III. The auxiliary constraint enhances accuracy performance, current magnitude error ($E_I\%$), and phase error (E_P) are below 4% and 4°, respectively. The increased measurement error compared with ideal conductors is due to the violation of the basic assumptions like straight conductors and perpendicular sensing plane. Given multiple nonidealities, the proposed approach is able to overcome individual sensor measuring error and achieve reasonably accurate solutions.

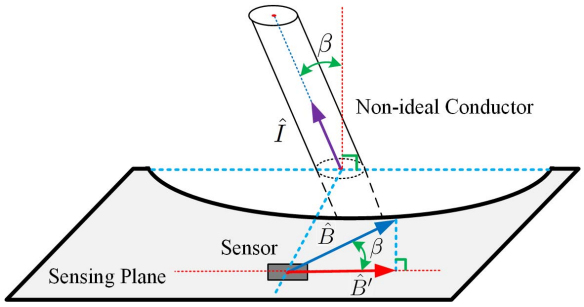

Fig. 14. Illustration of nonideal conductor directions.

E. Uncertainty Analysis

1) Conductor Directions: The 2-D model used in this paper assumes that all conductors are straight and perpendicular to the sensing plane shown in Fig. 2. This is guaranteed for the ideal conductor holder, but it may not be true for practical cables due to the following two nonidealities. First, the cable inside the conduit may not be perpendicular to the plane. Second, conductors may be rotating in the cable enclosure. Both the nonideal situations lead to a mismatch angle β as shown in Fig. 14. The sensors are only able to capture the projection component ofthe sensing plane $\hat{B}'$ as (10), instead of $\hat{B}$ generated by the current $\hat{I}$ of the nonideal conductor. A loss of $(1-\cos\beta)$ in sensed magnetic field is expected

$$\hat{B}' = \hat{B}\cos\beta. \tag{10}$$

In the practical example of household panel measurement, the length of conduit is at least 0.5 m and its internal diameter is 40 mm for a typical North American home. Assuming the cable is stiff, the maximum β is $\tan^{-1}(0.04/0.5) = 4.57°$. This indicates a maximum error of $(1-\cos 4.57°) = 0.32\%$ for the sensor voltages.

2) Dimensions of Conductors and Sensors: Both the dimensions of coil sensor and cable wire are actually not neglectable compared with the conduit diameter. However, they are assumed as dimensionless points in the 2-D model shown in Fig. 2, so that we are enabled to use (2) to build the formulation, instead of a complete finite element method analysis [11]. This uncertainty causes errors in sensor output voltages which almost linearly increase with reference currents, shown in Table II. Given the test bed setup, numerical simulations indicate that the impact of nonuniform magnetic field on the nonconcentric sensor model is found below 1% in sensor output voltage error, given the sensor-conductor distance is above 10 mm.

3) Sensor Noise and External Interference: Sensor noise is commonly modeled using a Gaussian distribution and contributes to the uncertainties in voltage phasor $V_{c,r}^k + \mathbf{i}V_{c,i}^k$ [11]. It is not significant as a current-independent uncertain factor according to E_V in Table II. External interference at power frequency is another critical issue of uncertainty; methods

have been developed to utilize spatial harmonic expansion to estimate external unknown magnetic sources and remove their impacts [20]. In the studied household panel measurement application, interference can be caused by the ac currents on outgoing wires near the sensing device. Since outgoing wires commonly have two hot wires with currents of opposite directions, most of their induced magnetic fields are canceled out given the relatively large distance between outgoing wires and sensors. The error in sensor output voltages caused by nearby outgoing wire interference is estimated to be below 2% for a typical home panel setup verified in the Appendix.

4) Amplifier Circuit and ADC: Interference on amplifier circuit may cause harmonics in output voltage waveforms, which are filtered out in Fourier transformation. Non-nominal parameters of circuit components do not cause errors for final results, since they are measured in the calibration process and accurately aggregated in gain factor ρ_k and phase shift ϕ_k. The errors caused by ADC are mainly in effect when output voltages are small in magnitude. For example, gathered conductor configuration with 2-A current shown in Table II leads to output voltages as small as 20 mV. The minimum recognizable signal step of 0.31 mV may result in $(0.31/20) = 1.55\%$ error in acquired voltage values.

5) Calibrating Conductor Positions: Uncertainty also exists in calibrating conductor positions, which are known parameters in calibration NLLS formulation (5). The errors in conductor positions affect the accuracy of the calibration results. The average diameter of the aluminum rod used for calibration is 3.618 mm and the diameter of the conductor hole is 4 mm, set in the 3-D printing model. Therefore, the maximum mismatch between the conductor center and the hole center is $((4 - 3.618)/2) = 0.191$ mm, which is the maximum error in conductor position parameters. Then, the sensitivity matrix of the calibration equations is calculated and the maximum value is found to be in the position of x_S^{12} with respect to x_C^6, with the value 2.461. This indicates a worst case that the error of 0.191 mm in the sixth conductor x-axis position will cause an error of $2.461 \times 0.191 = 0.470$ mm in the calibration result of 12th sensor x-axis position. No significant accuracy loss is found in current measurement tests after applying this error on the calibration results, thus, we believe this uncertainty issue is acceptable for the studied cases.

6) Ill-Condition Issue: Ill-condition issue refers to the situation that the solution of conductor currents are highly sensitive to the input parameters in solving (7). Thus, small measurement variations may lead to large variations in the solution of currents. To address this concern, a sensitivity analysis is performed to calculate the derivatives of conductor currents with respect to sensor voltages using reference values. Take Case 1 in Table I for example, the maximum value in the sensitivity matrix is found to be 13.390. Considering the worst case with sensor measurement error E_V as 83.05 mV (the maximum E_V in Table I), the resultant error is 4.63% for calculated current and acceptable for the investigated current measurement application. Considering the nature of Gaussian distribution in individual sensor error, the impact of ill-condition issue can be further reduced when multiple sensors are available.

TABLE IV
COMPUTING PERFORMANCE AND SOLUTION QUALITY

NLLS Formulation	Calibration (5)	Measurement (7)
Variables	14	84
Equality Const.	10	72
Inequality Const.	13	96
Observations (m)	10	24
Unknowns (n)	4	12
CPU Time (sec)	0.001	0.032
IPM Iterations	8	42
Objective Value	$1.1215e^{-4}$	$1.2611e^{-4}$
Feasibility Error	$4.18e^{-14}$	$5.53e^{-8}$
Optimality Error	$1.17e^{-8}$	$7.37e^{-11}$

F. Computing Performance

Based on the small dimension of the NLLS formulations for both calibration (5) and measurement (7), most of mainstream NLP solvers are able to solve them with promising efficiency and optimality. Table IV lists the scale of NLLS formulations and typical computational performance statistics. This indicates minor computing burden of the proposed approach; it is technically feasible to migrate this approach to portable embedded devices with real-time processing performance.

VII. CONCLUSION

A flexible and efficient method is developed to contactlessly measure currents for enclosed multiconductor systems using sensor array. The contribution is to set up a two-stage scheme of off-site sensor calibration and on-site current measurement, which simplifies measuring procedures and increases accuracy. The off-site calibration identifies sensor parameters which are independent of conductor configurations and valid for various measuring scenarios. Conductor currents and positions are then determined simultaneously in on-site measurement. The effectiveness of this approach is verified using ideal conductor and practical cable with satisfactory accuracy.

Future topics include extensions on other application scenarios, including Romex cables, distribution overhead lines, and so on. As an enabling technology for NILM, a harmonic current identification method will be developed, based on the conductor positions obtained in this paper using power frequency component. Also, further investigations will focus on accuracy improvement, including methods to eliminate external magnetic field interference in real-world environment.

APPENDIX
EXTERNAL INTERFERENCE EVALUATION

External magnetic field interference is identified as one of the common uncertainties in the measurements related to magnetic field. In this appendix, a worst case study is performed to evaluate the impact of external interference in the application of home electric panel measuring shown in Fig. 15. The U-shaped sensing device is to be installed around the conduit above the panel, where the incoming wires are inside. As we can see, there are multiple outgoing wires near the conduit, generating undesired interference magnetic fields.

The following laboratory experiments emulate a possible worst case of external interference impact by outgoing wires

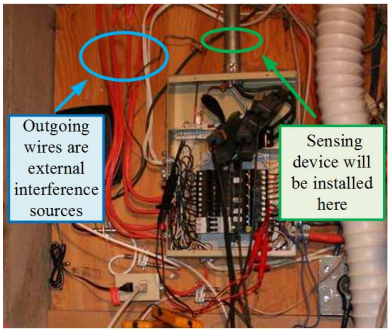

Fig. 15. Illustration of external interference source in home panel measurement.

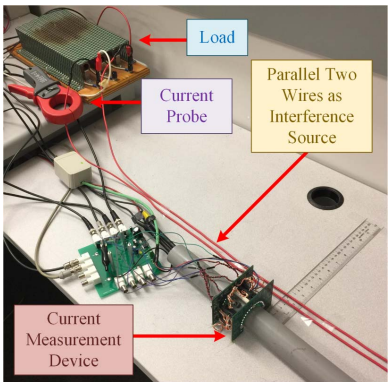

Fig. 16. Laboratory experiment of external interference evaluation.

TABLE V
IMPACT OF EXTERNAL INTERFERENCE EMULATED BY TWO PARALLEL WIRES

Distance (cm)	ΔE_V (mV)	$\Delta E_V\%$	E_I (A)	$E_I\%$	E_P (deg)
20	2.26	0.39%	0.41	1.71%	1.09°
15	6.41	0.69%	0.24	1.01%	0.92°
10	32.36	1.91%	0.51	2.17%	0.98°
5	243.36	11.76%	1.22	5.13%	4.48°

nearby, as shown in Fig. 16. The wire-to-wire distance of a pair of parallel outgoing wires is assumed as 10 mm and the outgoing currents on the wires are set as 10 A, which are typical values for home electric circuits. The maximum absolute and relative error in sensor voltages generated by the outgoing wires are shown as ΔE_V and $\Delta E_V\%$ in Table V, respectively, given different wire-to-sensor distances in a typical cable test as Table III. Similarly, the absolute and relative current measurement errors are shown in the columns of E_I and $E_I\%$, respectively. This result indicates the impact of external interference in the studied case that is acceptable as long as the outgoing wires are more than 10 cm away. The proposed approach is able to achieve similar measuring performance as Table III under the emulated external interference.

ACKNOWLEDGMENT

All the experiments were performed at the Department of Electrical and Computer Engineering, University of Alberta. The authors would like to thank Dr. J. Yong, Dr. X. Yang, and P. Gao for fruitful discussions.

REFERENCES

[1] S. Ziegler, R. C. Woodward, H. H.-C. Iu, and L. J. Borle, "Current sensing techniques: A review," *IEEE Sensors J.*, vol. 9, no. 4, pp. 354–376, Apr. 2009.
[2] J. M. Libove and J. R. Singer, "Apparatus for measuring voltages and currents using non-contacting sensors," U.S. Patent 5 473 244, Dec. 5, 1995.
[3] X. Sun, Q. Huang, Y. Hou, L. Jiang, and P. W. T. Pong, "Noncontact operation-state monitoring technology based on magnetic-field sensing for overhead high-voltage transmission lines," *IEEE Trans. Power Del.*, vol. 28, no. 4, pp. 2145–2153, Oct. 2013.
[4] J. N. Sharood, G. Bailey, D. M. Carr, J. Turner, and D. Peachey, "Appliance retrofit monitoring device with a memory storing an electronic signature," U.S. Patent 6 934 862, Aug. 23, 2005.
[5] G. W. Hart, "Nonintrusive appliance load monitoring," *Proc. IEEE*, vol. 80, no. 12, pp. 1870–1891, Dec. 1992.
[6] J. Lenz and A. S. Edelstein, "Magnetic sensors and their applications," *IEEE Sensors J.*, vol. 6, no. 3, pp. 631–649, Jun. 2006.
[7] J. D. Bull, N. A. F. Jaeger, and F. Rahmatian, "A new hybrid current sensor for high-voltage applications," *IEEE Trans. Power Del.*, vol. 20, no. 1, pp. 32–38, Jan. 2005.
[8] K. Draxler, R. Styblikova, J. Hlavacek, and R. Prochazka, "Calibration of Rogowski coils with an integrator at high currents," *IEEE Trans. Instrum. Meas.*, vol. 60, no. 7, pp. 2434–2438, Jul. 2011.
[9] K.-L. Chen and N. Chen, "A new method for power current measurement using a coreless Hall effect current transformer," *IEEE Trans. Instrum. Meas.*, vol. 60, no. 1, pp. 158–169, Jan. 2011.
[10] C.-T. Liang, K.-L. Chen, Y.-P. Tsai, and N. Chen, "New electronic current transformer with a self-contained power supply," *IEEE Trans. Power Del.*, vol. 30, no. 1, pp. 184–192, Feb. 2015.
[11] G. D'Antona, L. Di Rienzo, R. Ottoboni, and A. Manara, "Processing magnetic sensor array data for AC current measurement in multiconductor systems," *IEEE Trans. Instrum. Meas.*, vol. 50, no. 5, pp. 1289–1295, Oct. 2001.
[12] M. Bourkeb *et al.*, "Device for measuring currents in the conductors of a sheathed cable of a polyphase network," WO Patent 2013 068 360 A1, May 16, 2013.
[13] AVO International Limited. *Megger FlexiClamp 200 User Guide*, accessed on Jan. 20, 2017. [Online]. Available: http://www.biddlemegger.com/biddle-ug/Flexiclamp_200_UG.pdf
[14] P. Gao, S. Lin, and W. Xu, "A novel current sensor for home energy use monitoring," *IEEE Trans. Smart Grid*, vol. 5, no. 4, pp. 2021–2028, Jul. 2014.
[15] *Energy Inc.'s the Energy Detective (TED), Specifications of TED Spyder*, accessed on Jan. 20, 2017. [Online]. Available: http://www.theenergydetective.com/downloads/spyderspec.pdf
[16] AEMC Instruments. *AC Current Probe Model MN252*, accessed on Jan. 20, 2017. [Online]. Available: http://www.aemc.com/products/pdf/2115.78.pdf
[17] R. Fourer, D. M. Gay, and B. W. Kernighan, *AMPL: A Modeling Language for Mathematical Programming*. Boston, MA, USA: Cengage Learning, 2002.
[18] R. H. Byrd, J. Nocedal, and R. A. Waltz, "KNITRO: An integrated package for nonlinear optimization," in *Large-Scale Nonlinear Optimization*. New York, NY, USA: Springer, 2006, pp. 35–59.
[19] J. Zhang, Y. Wen, and P. Li, "Nonintrusive current sensor for the two-wire power cords," *IEEE Trans. Magn.*, vol. 51, no. 11, Nov. 2015, Art. no. 4005304.
[20] L. D. Rienzo and Z. Zhang, "Spatial harmonic expansion for use with magnetic sensor arrays," *IEEE Trans. Magn.*, vol. 46, no. 1, pp. 53–58, Jan. 2010.

Guangchao Geng (S'10–M'14) received the B.S. and Ph.D. degrees in electrical engineering from the College of Electrical Engineering, Zhejiang University, Hangzhou, China, in 2009 and 2014, respectively.

He is currently a Post-Doctoral Fellow with the College of Control Science and Engineering, Zhejiang University, and with the Department of Electrical and Computer Engineering, University of Alberta, Edmonton, AB, Canada. His current research interests include power disturbance analytics, power system stability and control, and renewable energy integration.

Juncheng Wang (S'15) received the B.S. degree in electrical engineering from Shanghai Jiao Tong University, Shanghai, China, in 2014. He is currently pursuing the master's degree with the Department of Electrical and Computer Engineering, University of Alberta, Edmonton, AB, Canada.

His current research interests include smart grid and adaptive sensor array technique.

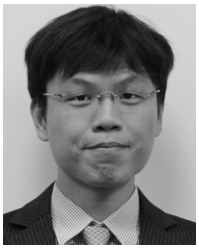

Kun-Long Chen (S'11–M'15) received the B.S.E.E. degree from Feng-Chia University, Taichung, Taiwan, in 2004, and the M.S.E.E. and Ph.D. degrees from the National Taiwan University of Science and Technology, Taipei, Taiwan, in 2006 and 2011, respectively.

He is currently a Post-Doctoral Fellow with the Department of Electrical and Computer Engineering, University of Alberta, Edmonton, AB, Canada. His current research interests include nonconventional voltage and current sensors, power metrology for smart grid, and nonintrusive load monitoring system.

Wilsun Xu (M'90–SM'95–F'05) received the Ph.D. degree from the University of British Columbia, Vancouver, BC, Canada, in 1989.

He is currently an NSERC/iCORE Industrial Research Chair Professor with the University of Alberta, Edmonton, AB, Canada. His current research interests include power quality, power disturbance analytics, and power system measurements.